PNAS RESEARCH ARTICLE | GENETICS OPEN ACCESS

rDNA array length is a major determinant of replicative lifespan in budding yeast

Manuel Hotz[a,1], Nathaniel H. Thayer[a,1], David G. Hendrickson[a,1], Elizabeth L. Schinski[a], Jun Xu[a], and Daniel E. Gottschling[a,2]

Contributed by Daniel Gottschling; received October 27, 2021; accepted March 1, 2022; reviewed by Andreas Hochwagen and Jeffrey Smith

The complex processes and interactions that regulate aging and determine lifespan are not fully defined for any organism. Here, taking advantage of recent technological advances in studying aging in budding yeast, we discovered a previously unappreciated relationship between the number of copies of the ribosomal RNA gene present in its chromosomal array and replicative lifespan (RLS). Specifically, the chromosomal ribosomal DNA (rDNA) copy number (rDNA CN) positively correlated with RLS and this interaction explained over 70% of variability in RLS among a series of wild-type strains. In strains with low rDNA CN, *SIR2* expression was attenuated and extrachromosomal rDNA circle (ERC) accumulation was increased, leading to shorter lifespan. Suppressing ERC formation by deletion of *FOB1* eliminated the relationship between rDNA CN and RLS. These data suggest that previously identified rDNA CN regulatory mechanisms limit lifespan. Importantly, the RLSs of reported lifespan-enhancing mutations were significantly impacted by rDNA CN, suggesting that changes in rDNA CN might explain the magnitude of some of those reported effects. We propose that because rDNA CN is modulated by environmental, genetic, and stochastic factors, considering rDNA CN is a prerequisite for accurate interpretation of lifespan data.

aging | ribosomal DNA | *Saccharomyces cerevisiae* | machine learning | microfluidics

Significance

Genes encoding ribosomal RNA (rDNA) are organized into a repetitive array in eukaryotic genomes. The copy number of these genes often varies and is responsive to genetics and environment. Here, we show that variation in copy number at the rDNA locus is capable of altering replicative lifespan in yeast. These results indicate that considering rDNA copy number, and conditions that could potentially change this dynamic chromosome locus, is critical for evaluating lifespan. We propose that this rDNA locus represents the kind of repeated element in eukaryotic genomes that escapes easy detection, yet has phenotypic consequences, in this case lifespan.

Budding yeast, *Saccharomyces cerevisiae*, has been a foundational model organism for the study of cellular aging. Cells divide asymmetrically and the mother cell undergoes a limited number of divisions, which defines the cell's replicative lifespan (RLS). Measuring RLS is technically challenging and only recent advances have enabled more efficient screening for lifespan-modulating factors (1–5).

A number of processes, pathways, and mechanisms have been implicated in yeast aging (reviewed in ref. 6), with regulators of the ribosomal RNA gene array (rDNA) representing perhaps the best-characterized group of lifespan modulators. Proteins that act at the rDNA locus modify rDNA stability and the formation of extrachromosomal rDNA circles (ERCs), a known aging factor in *S. cerevisiae* (7). Sir2, the defining member of the Sirtuin family of histone deacetylases, silences the rDNA locus and suppresses formation of ERCs (8). Conversely, the protein Fob1 binds to a replication fork barrier site in the rDNA locus, decreases rDNA stability, and thus promotes the production of ERCs (9, 10). Since the accumulation of ERCs in the mother cell limits its RLS, *sir2*Δ and *fob1*Δ strains are short and long lived, respectively (8, 11).

The rDNA locus is highly repetitive and dynamic. While 150 repeats are considered a normal copy number (CN) for the strain background used in this study, the number of repeats commonly ranges from 100 to 250 copies (12). And while the size of the rDNA array is relatively stable for a limited number of divisions, rDNA CN can change on a timescale faster than the estimated mutation rate (13). Thus, it may be considered a type of "contingency locus," which is characterized by environmentally responsive genetic variation that results in distinct phenotypic outcomes (14–16).

The rDNA copy number varies significantly in strains found in the wild and those used in the laboratory (12, 13, 17–19). This variation can occur spontaneously, but can also be introduced by standard laboratory DNA transformation protocols or changes in growth environment (12, 13, 20). In addition, there are Sir2- and Fob1-dependent feedback mechanisms in place by which a "normal" rDNA CN is maintained through modulation of Sir2 expression levels (21). Interestingly, rDNA array size is anticorrelated with ERC abundance in young cells, suggesting that chromosomal and extrachromosomal rDNA are in an equilibrium (13). Despite this known connection between rDNA array size and Sir2 and ERC levels, no evidence for array size impacting lifespan has been found (12, 15, 18).

Yet, significant variability exists within reported lifespans of *S. cerevisiae*. A metastudy found that the RLS of the same wild-type strains varied between 20 and 40, depending on the study in which it was reported (22). This variability was attributed to a reporting bias and small sample sizes. However, these findings are also consistent with uncontrolled

Author affiliations: [a]Calico Life Sciences LLC, South San Francisco, CA 94080

Author contributions: M.H., N.H.T., D.G.H., and D.E.G. designed research; M.H., N.H.T., D.G.H., and E.L.S. performed research; M.H., N.H.T., D.G.H., and J.X. analyzed data; and M.H., N.H.T., D.G.H., and D.E.G. wrote the paper.

Reviewers: A.H., New York University; and J.S., University of Virginia.

Competing interest statement: M.H., N.H.T., D.G.H., E.L.S., J.X., and D.E.G. are employees of Calico Life Sciences LLC. The work presented here is not of commercial value to Calico, but rather a contribution to advancing the study of yeast aging.

See online for related content such as Commentaries.

[1]M.H., N.H.T. and D.G.H. contributed equally to this work.

[2]To whom correspondence may be addressed. Email: dang@calicolabs.com.

This article contains supporting information online at https://www.pnas.org/lookup/suppl/doi:10.1073/pnas.2119593119/-/DCSupplemental.

Published April 8, 2022.

genetic or environmental factors contributing to the variability. In addition, a genome-wide screen measuring the RLS of deleted nonessential genes found a significant discrepancy between strains with opposing mating types carrying the same gene deletion (23). This discrepancy was mostly attributed to statistical error due to a low number of cells analyzed, but was not fully explored. Given this large degree of variability, which likely impacts the interpretation of any lifespan measurement, we wanted to address the underlying cause. Here we show that the chromosomal rDNA copy number is an important determinant of replicative lifespan in yeast and can explain a large part of the reported variability in lifespan.

Results

rDNA Array Length Strongly Correlates with Replicative Lifespan of Wild-Type Strains. A recently developed microfluidic system, which uses automated hardware and a machine-learning algorithm for analysis (1), was employed to obtain large quantities of RLS data for an extended series of wild-type yeast strains. Although these strains were derived from the same diploid parent strain, dramatic variability in RLS was observed (Fig. 1*A*, spontaneous variation). This phenomenon has been previously reported, but the underlying cause has largely remained unknown (22).

To address whether genetic differences might explain the observed variability in lifespan, whole-genome sequencing (WGS) was performed and the lifespan data were compared with the occurrence of single-nucleotide polymorphisms (SNPs) and other types of polymorphisms (Fig. 1 *B* and *C*). Among all SNPs and copy number variations (CNVs), the clearest signal correlating with lifespan came from the rDNA locus, which showed a gradual increase in CN along with enhanced median RLS. To test the validity of rDNA CN estimates obtained by WGS, the size of the rDNA arrays was confirmed by electrophoresis of intact arrays (contour-clamped homogeneous electric-field electrophoresis [CHEF]) (*SI Appendix*, Fig. S1).

To further examine the impact of rDNA CN on lifespan, a large series of wild-type strains with variable rDNA CNs were constructed by two different means (Fig. 1 *D* and *E*, experimental variation). First, a diploid wild-type strain was sporulated to spontaneously create variability. Second, to obtain strains with more extreme CNs, a construct replacing random numbers of rDNA repeats was introduced (*Materials and Methods*) (13). When assessing lifespans for this entire panel of strains and comparing it to rDNA CN, there again was a strong correlation between the two in strains with CNs <150 repeats, while CNs above 150 did not increase RLS any further. Cox proportional hazard estimates indicate that each loss of 10 rDNA repeats (below 150) results in a $20 \pm 0.2\%$ increase in hazard (95% confidence interval), explaining over 70% of variation observed in median lifespan. In summary, a large part of the variability in lifespan among these wild-type strains is explained by differences in rDNA CN.

Environment and genetics can impact many phenotypes, including RLS (24). This led us to ask whether the correlation between lifespan and rDNA array length was also observed under different growth conditions and genetically different strains. Lifespan experiments and CN estimation in three different media types were performed: minimal medium, synthetic complete medium (contains amino acids, etc.), and rich medium (see *Materials and Methods*). Under these conditions, there was again a strong correlation between CN and lifespan (*SI Appendix*, Fig. S2). In addition, it is worth noting that while the correlation remains strong in all three media, growth in YNB generally produced longer RLS for a given rDNA CN and YPD a shorter RLS. Together with the observation that the impact of rDNA CN on RLS was similar in a another strain (25) (*SI Appendix*, Fig. S3), we conclude that rDNA CN impacts RLS under multiple disparate scenarios. Finally, we confirmed that rDNA CN impacts RLS when lifespan was measured with the traditional microdissection assay (*SI Appendix*, Fig. S4) (26).

ERC and Sir2 Levels Underlie the Positive Correlation between Lifespan and rDNA Array Size. During log-phase growth of yeast cells, there is a dynamic equilibrium between ERCs and the number of chromosomal rDNA copies (13). ERC levels anticorrelate with rDNA CN, but no further connection to aging and lifespan has been established. To test whether ERC levels were affected by rDNA CN in aging cells, a modified version of the miniature-chemostat aging device (MAD) (*Materials and Methods*) (27) was used to obtain large numbers of aged cells ($\sim 6 \times 10^8$ cells per sample). Seven wild-type strains with variable rDNA CNs were aged for 24 h, the total DNA was extracted to run on an agarose gel, and a Southern blot was performed to detect both forms of rDNA (the chromosomal array and ERCs; Fig. 2 *A* and *B*). As a control, seven *fob1*Δ strains of comparable rDNA CNs were included, a mutant in which ERC levels are drastically reduced, because ERC accumulation during aging is attenuated (11). In samples from aged wild-type cells, ERCs appeared in more than four isoforms (labeled 1 to 4 in Fig. 2*A*), a similar pattern to that previously described (13, 28). These isoforms were strongly reduced in the aged *fob1*Δ controls (Fig. 2*A*), as well as in young cells (*SI Appendix*, Fig. S5). When ERC levels were quantified by integrating the signal from all major species, a strong anticorrelation between ERC levels and rDNA CN in wild-type strains was observed (Fig. 2*B*). Consistent with lifespan (Fig. 1*E*), ERC levels did not decrease any further in strains with rDNA CN >150. In contrast to wild type, ERC levels remained low in *fob1*Δ strains, irrespective of rDNA array length or age. These data suggest that ERC accumulation with age is dramatically higher in wild-type cells with short rDNA arrays, which may explain why these cells have shortened lifespans.

To examine this phenomenon via another cellular phenotype, we took advantage of the large collection of time-lapse movies obtained with our microfluidic system. Previous studies have reported that yeast cells follow distinct aging trajectories, with one fraction of the population dying from rDNA/ERC-related causes and the other dying via rDNA-independent paths (mitochondrial defects, etc.) (29, 30). These two subpopulations are readily distinguishable by cell morphology, with the rDNA-related trajectory showing an elongated daughter cell morphology prior to death and the rDNA-independent trajectory correlating with round daughter cell shape. Using this phenomenon, cells were categorized by their mode of death (MoD) by distinguishing between an "rDNA-dependent MoD" and an "rDNA-independent MoD" with a machine-learning algorithm (*SI Appendix*, Fig. S6; see *Materials and Methods* for details). When calculating the hazard risk (chance of a cell to die within a division) for each of these strains, we noticed that the hazard risk increased drastically at earlier divisions in cells with lower rDNA CN (Fig. 2*C*). Importantly, this increased risk of dying was predominantly observed in cells of the rDNA-related MoD category, indicating that it was due to rDNA- and ERC-dependent causes of death. In contrast, other cellular phenotypes associated with lifespan, such as growth rate and cell size (31, 32), did not show a meaningful correlation with RLS in the strains examined (*SI Appendix*, Figs. S7 and S8).

If ERCs play a critical role for shortening lifespan and increasing hazard risk in cells with short rDNA arrays, reducing the number of ERCs should restore long lifespan even in strains

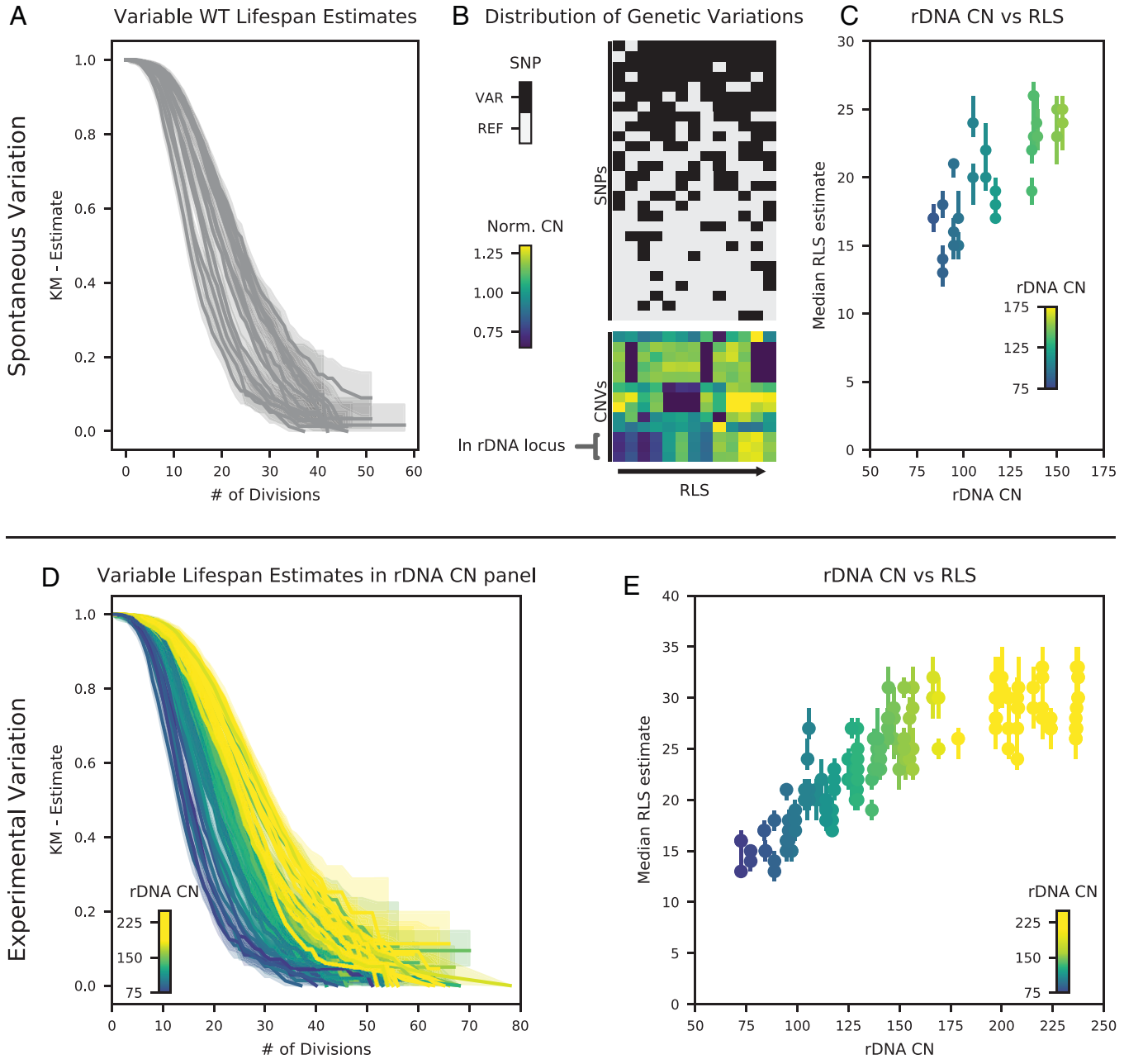

Fig. 1. rDNA copy number explains a majority of the variability in RLS estimates. (*A*) Kaplan–Meier estimates for 13 wild-type strains derived from the same parent show significant variability ("spontaneous variation"; >400 observations per curve, median of ∼1,000 observations per curve, 95% confidence interval represented by shaded region). (*B*) Copy number variations in the rDNA locus correlate with RLS. Polymorphisms identified by whole-genome sequencing data are grouped into SNPs and CNVs of 2-kb genome bins. Forty-one polymorphisms occurring in at least two strains are shown. Strains are ordered by increasing median RLS from left to right. Color map for SNPs is gray (absent, REF) and black (present, VAR). Color map for CNVs is from low (dark blue) to high (yellow). (*C*) rDNA CN correlates with median RLS. Color map indicates rDNA CN and is maintained throughout the rest of the plots. Each point represents a unique lifespan experiment (microfluidic channel) with >400 cells. Ninety-five percent confidence intervals around median RLS estimate are represented as vertical bars. (*D*) Kaplan–Meier estimates for an extended panel of 54 wild-type strains with variable rDNA CN ("experimental variation"; >400 observations per curve, median ∼1,150 observations per curve). (*E*) Correlation of median RLS and rDNA CN for the same strains as in *D* (n = >319 per microfluidic channel, median 593 cells).

with low rDNA CN. To evaluate this idea, lifespans of a panel of *fob1*Δ strains were measured, where ERC abundance was low regardless of rDNA CN (Fig. 2 *A* and *B*). In contrast to wild-type cells, *fob1*Δ cells were long lived irrespective of rDNA CN in strains with as few as 35 rDNA repeats and no correlation with rDNA CN was observed (Fig. 2*D*). In addition, *fob1*Δ strains did not show the characteristic inverse correlation of hazard rate with rDNA CN among cells with rDNA-related MoD that is apparent in wild-type strains (Fig. 2*C*). Together, these data strongly suggest that the enhanced accumulation of ERCs in strains with low rDNA CN is the underlying cause for the inverse correlation between rDNA CN and lifespan.

Iida and Kobayashi (21) proposed that the upstream activating factor (UAF) complex of the rRNA gene can also act as a transcriptional repressor at the *SIR2* locus. They suggest that there is a competition for limiting UAF between the rDNA and *SIR2* loci. Occupancy at the *SIR2* locus increases with low rDNA CN and as a result, there is reduced expression of Sir2. This model could explain why ERC levels are higher and lifespan is shorter in cells with reduced chromosomal rDNA CN. To test whether

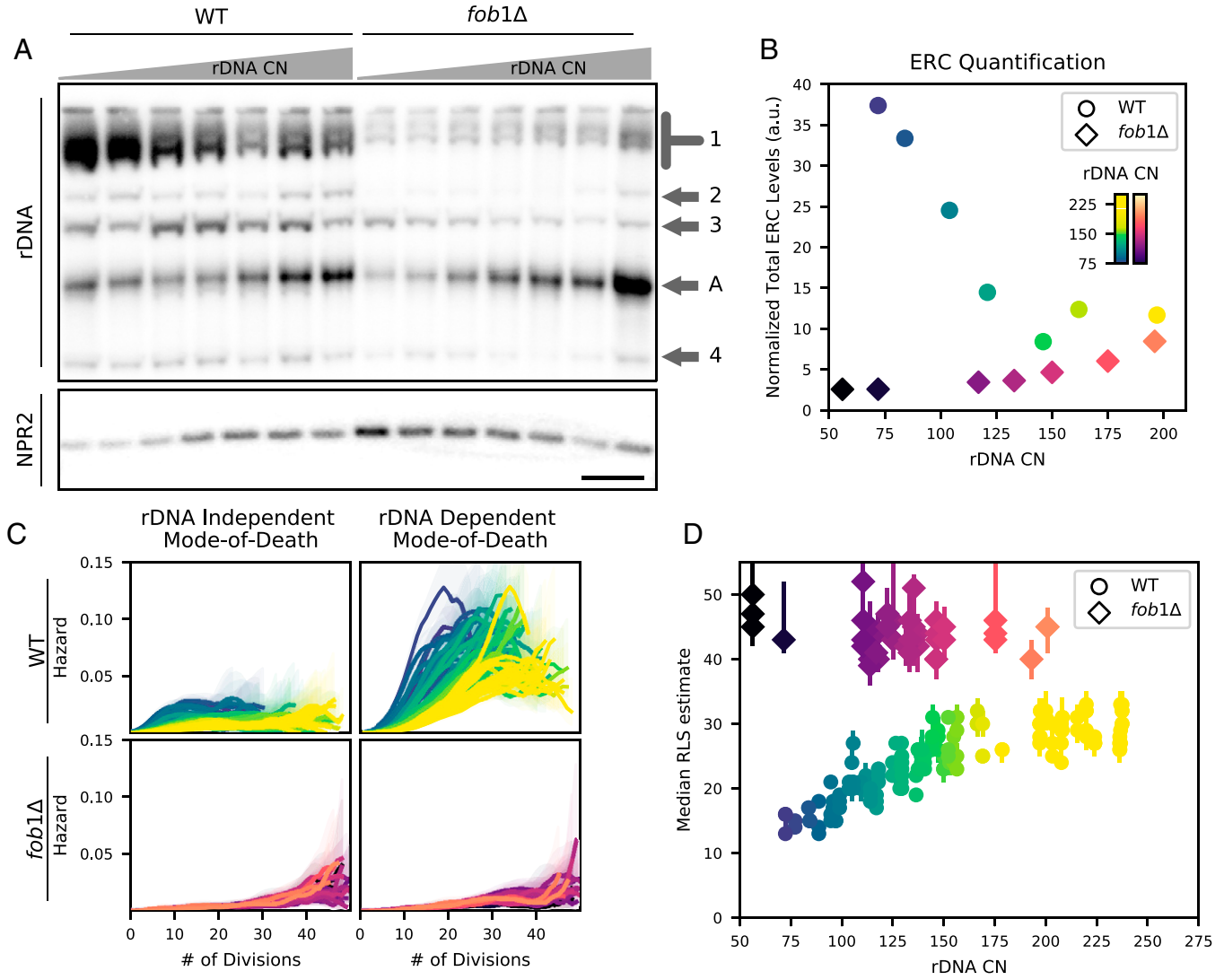

Fig. 2. Chromosomal rDNA CN modulates lifespan via ERC levels. (*A*) Southern blots probed for rDNA and *NPR2* (loading control). Samples were obtained from wild-type and *fob1*Δ strains with variable rDNA CN aged for 24 h. Arrows 1 to 4 highlight bands of ERCs, and arrow A highlights the chromosomal rDNA array. (Scale bar, 1 cm.) (*B*) Quantification of ERCs on blot from *A* shows anticorrelation between rDNA CN and ERC levels. ERC accumulation is suppressed by deletion of *FOB1*. Sum intensity of all four ERC bands is plotted. (*C*) Hazard estimates for 51 wild types and 20 *fob1*Δ strains derived from microfluidics experiments show increased hazard risk for cells in rDNA-dependent MoD with low rDNA CN. This effect is suppressed by *fob1*Δ. Color maps, indicating rDNA CN, are the same as in *B* (>400 cells per hazard estimate; shaded regions represent 95% confidence interval). (*D*) *fob1*Δ eliminates the correlation between rDNA CN and RLS (>400 cells per median lifespan estimate; vertical bars represent 95% confidence interval).

the *SIR2* locus was indeed altered by rDNA CN, the Assay for Transposase-Accessible Chromatin using Sequencing (ATAC-Seq) was performed on the panel of wild-type strains. As predicted, a region immediately upstream of *SIR2*, which is a known binding site for UAF (21), was more accessible with reduced rDNA CN (Fig. 3 *A* and *B*). In addition, gene expression was examined via RNA-Seq using traditional polyadenylated (polyA) RNA selection. While there was a small set of genes that were altered by rDNA CN, the gene most correlated was *SIR2*, consistent with previous reports (15, 21). Furthermore, when gene expression was examined as a function of lifespan, rather than rDNA CN, *SIR2* was the gene most correlated with RLS (Fig. 3*C*). Together, these data suggest that the predominant effect of higher rDNA copy number is increased productive transcription at the *SIR2* locus resulting in reduced ERC formation and thus accumulation with age.

Since yeast cells are known to maintain rRNA expression constant despite differences in rDNA CN (33), we wanted to examine whether this was true in the strains used here. RNA-Seq on total RNA (without enriching for mRNA) was performed to measure the levels of rRNA relative to the rest of the transcriptome (*SI Appendix*, Fig. S9). There was no significant difference between the strains with variable rDNA CN, which is in agreement with previous results (33). Taken together, our results suggest that the predominant underlying effect of higher rDNA CN on lifespan is an increase in *SIR2* expression and reduced accumulation of ERCs.

rDNA Array Size Alters the Lifespan of Known Aging Modulators. There is abundant evidence that rDNA array size can vary dramatically from strain to strain within and between strain collections (12, 19, 34). For instance, strains from the commonly used yeast knockout (YKO) collection (35) had a wide distribution of rDNA CNs, carrying anywhere between 80 and 180 rDNA repeats (12). Given this wide range of rDNA CN and its effect on lifespan, we were curious about how much of an impact rDNA

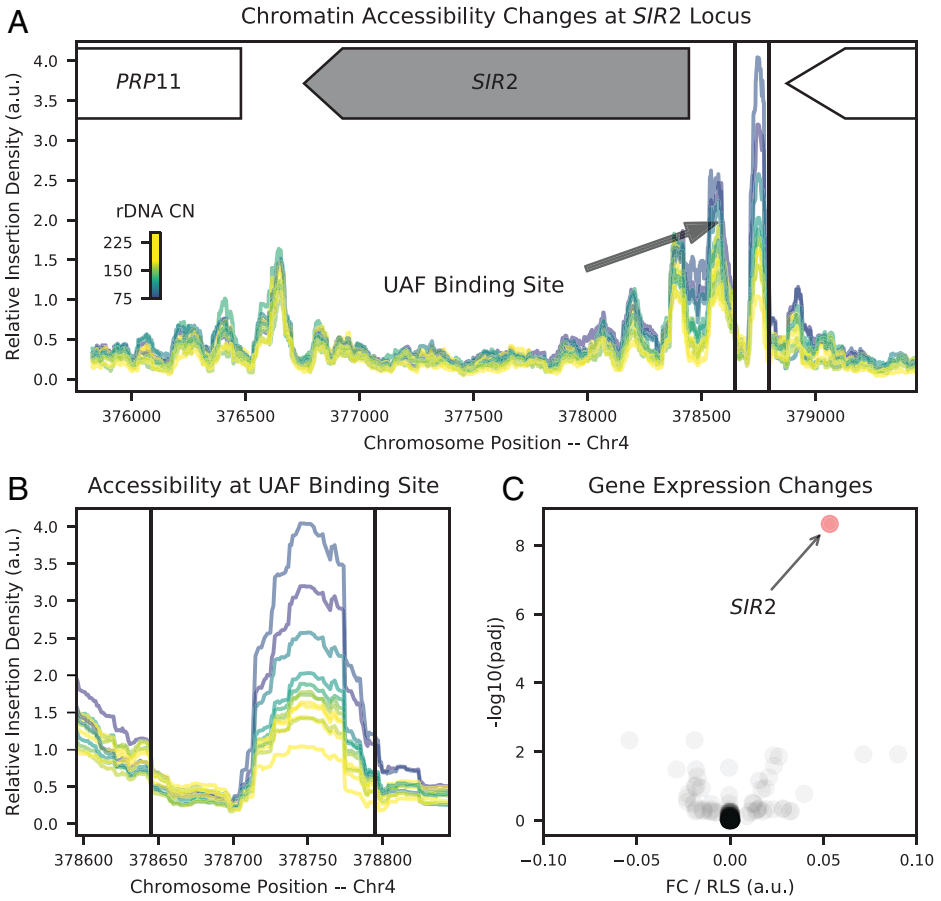

Fig. 3. *SIR2* accessibility and expression correlate with rDNA CN and RLS. (*A*) Chromatin accessibility at the *SIR2* locus as derived by ATAC-Seq. The UAF-binding site upstream of *SIR2* shows increased accessibility with decreasing rDNA CN. Color map is the same as in Fig 1. (*B*) Magnification of chromatin accessibility changes at the UAF-binding site from *A*. (*C*) Sir2 gene expression is strongly up-regulated with increasing RLS. Fold change of gene expression is plotted as a function of RLS (FC/RLS) vs. the adjusted *P* value [−log10(padj)].

CN had on the RLS of known lifespan modulators. To this end, panels of the following deletion mutants were created, each with varying rDNA CN: *gpa2*Δ, *idh1*Δ, *rpl13A*Δ, *ubp8*Δ, *hda2*Δ, *ubr2*Δ, and *tor1*Δ. These mutants span a range of processes implicated in aging and have previously been found to be long lived (23, 36–41).

When measuring the effect of each mutation on survival in the context of different rDNA CNs, three conclusions emerged (Fig. 4 *A*–*H*). First, the effect of rDNA array length on lifespan could be dramatic, even in the presence of a reported lifespan-enhancing mutation. Second, some of the mutants were indeed long lived relative to wild type at a normal rDNA CN (∼150). However, in other mutants no significant difference in RLS was detected at any copy number. Importantly, all of the lifespan-changing effects of the mutants were reliably observable and interpretable only when taking rDNA array length into account. Third, in some cases the relationship between rDNA CN and lifespan was modulated by the mutation. For example, the *fob1*Δ mutation attenuated the effect of rDNA CN on lifespan across the entire range of rDNA CNs, in agreement with ERC accumulation causing this effect. In contrast, *hda2*Δ exacerbated the relationship such that the effect of rDNA CN on lifespan was even greater than in wild type (WT). The *ubp8*Δ mutant also appeared to modulate this relationship, but to a lesser extent and possibly only over a limited range of rDNA CN. Together, these data strongly suggest that the rDNA CN is a parameter essential for the accurate interpretation of replicative lifespan data, in wild type as well as in various mutant backgrounds.

Discussion

In this study, we discovered that the number of repeats at the rDNA locus is a major determinant of RLS in *S. cerevisiae*. Strikingly, over 70% of variation in RLS between otherwise identical wild-type strains was explained by the number of rDNA copies on the chromosome (rDNA CN). Specifically, the median RLS increased by twofold, from ∼15 to ∼30 cell divisions, when the rDNA CN doubled from 75 to 150 copies (Fig. 1). Our results provide another level of understanding about RLS determination in budding yeast.

Furthermore, we offer a mechanistic explanation for this rDNA CN effect on RLS, which is consistent with all our data and builds upon important findings from others (Fig. 5). The CN of rDNA repeats within the chromosomal locus is in dynamic equilibrium with ERCs (13), a causal factor for reduced lifespan in *S. cerevisiae* (7). Strains with low rDNA CN and shorter lifespan have lower levels of Sir2 expression (15, 21) and as a result accumulate ERCs at a faster rate (Figs. 1 and 2). In support of this model, we recapitulate previous observations describing the effect of rDNA CN on the UAF binding site at the *SIR2* locus, *SIR2* transcription, and ERC formation (13, 21) and show the effect of ERC formation on mode of death and lifespan. Importantly, the effects of rDNA CN both on RLS and on ERC formation are completely ablated in a *FOB1* deletion background, where ERC formation is severely attenuated.

We observed an interaction between rDNA and RLS by generating a high-diversity rDNA copy number panel spanning from

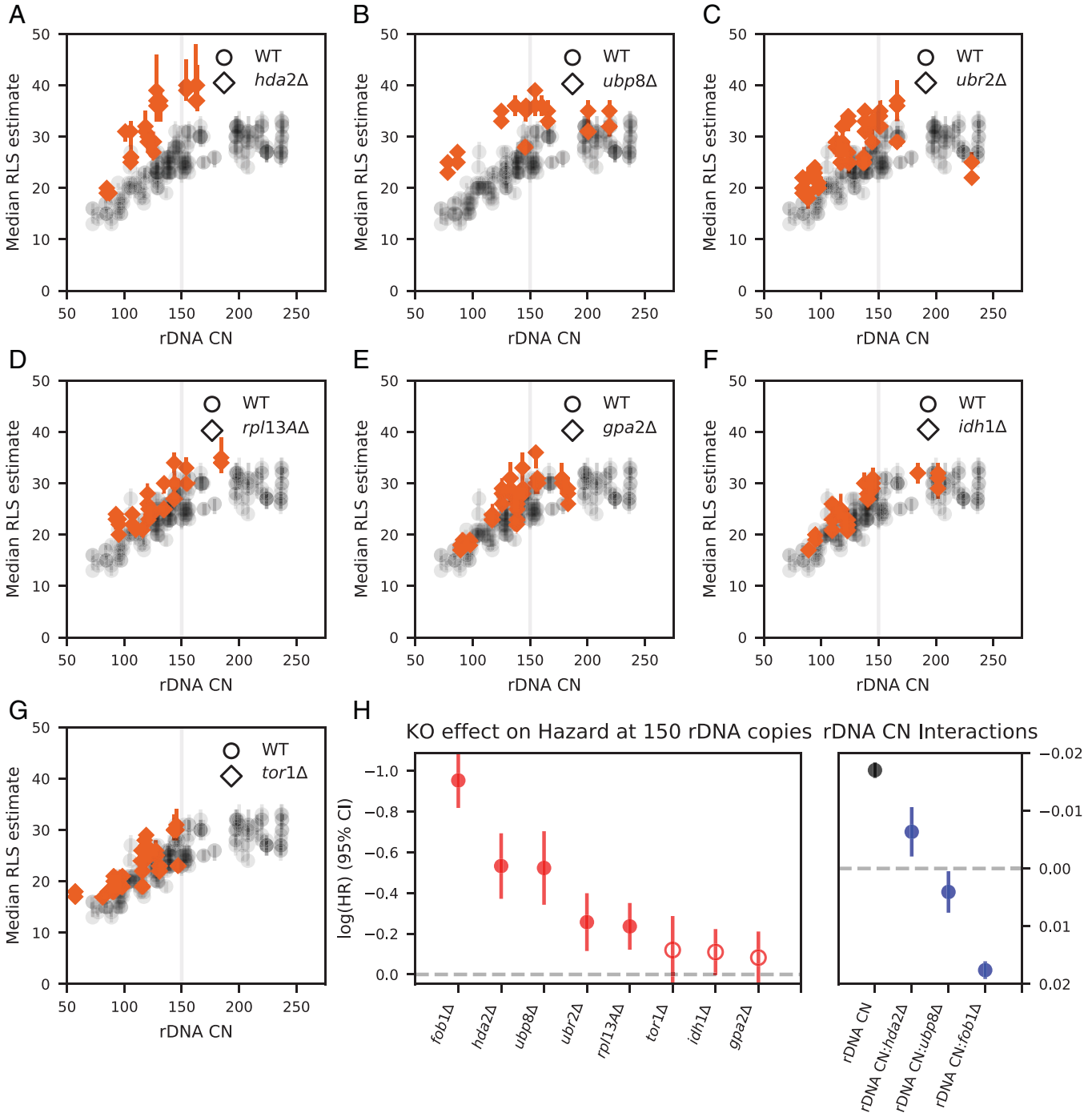

Fig. 4. rDNA CN affects the lifespan of known modulators of aging. (*A*–*G*) Correlation of median RLS and rDNA CN for wild-type and mutant strains as indicated (>300 cells per lifespan estimate; median = 593). Vertical gray line indicates rDNA CN of 150. (*H*) Cox Proportional Hazard model testing the effect of mutations on the hazard at 150 rDNA CN (*Left*) and on the correlation between rDNA CN and RLS (*Right*). (*H*, *Left*) Negative coefficients indicate a reduction in hazard due to the mutation at an rDNA CN of 150. Vertical bars represent 95% confidence interval, and open circles indicate that the estimated range overlaps with 0. (*H*, *Right*) More positive interaction terms indicate a weaker correlation between rDNA CN and RLS in the indicated mutant background. Coefficients are measured per mutation or per unit change for rDNA CN.

50 to 220 copies. In doing so, we were able to test the effect over a large copy number range and sample size using our high-throughput lifespan machines (1). We generated single-cell longitudinal lifespan data for >300,000 cells from >200 unique strains in >550 lifespan experiments and used high-throughput genotyping to accurately measure rDNA CN. These methods allowed for the effect of rDNA CN on yeast RLS to be discerned, which previous studies might have been underpowered to detect (12, 15, 18).

We propose that differences in rDNA CN could explain a significant amount of variation in lifespan reported in the literature (22), which has implications for interpreting previously reported lifespan effects in various mutant strains. We tested lifespans for a small set of such mutants, which all had been reported to extend RLS (23, 36–41). With the exception of *fob1*Δ, the chromosomal rDNA CN had a strong influence on lifespans of these mutants, particularly in the 75 to 150 copy number range (Fig. 4). And while some of the mutations indeed had an additive effect on

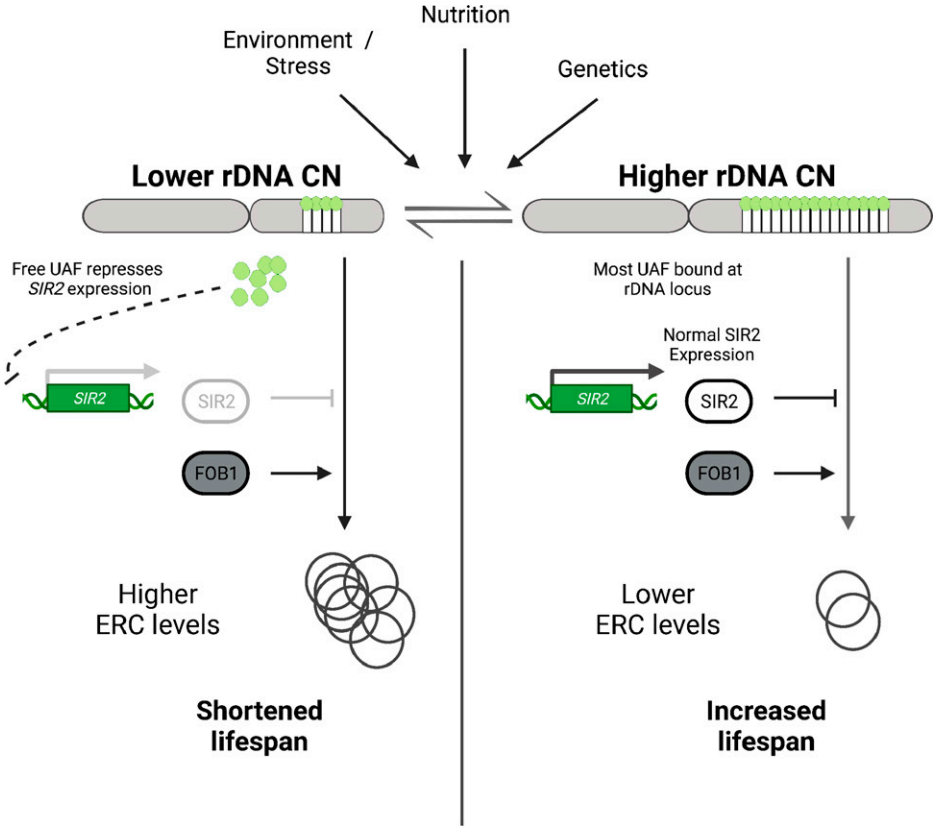

Fig. 5. rDNA CN affects lifespan through known regulation of established aging factors. Model shows how differences in rDNA CN affect lifespan. In cells with low rDNA CN, Sir2 expression is low due to repression by the UAF complex, which in turn causes ERC accumulation and shortens lifespan.

RLS at a defined rDNA CN (e.g., *hda2*Δ, *ubp8*Δ, and *ubr2*Δ), surprisingly, others did not (e.g., *tor1*Δ, *idh1*Δ, and *gpa2*Δ). While we cannot exclude that these deletions might have stronger effects in environments that were not tested in our microfluidic devices, we postulate that a longer rDNA array was the underlying reason for previously reported lifespan-extending effects.

There are several ways by which mutant strains could have had a different rDNA CN in an RLS study compared to their corresponding wild-type control strain. First, genome manipulations, such as transformations typically used to introduce a mutant allele, can alter the chromosomal rDNA CN (12). Second, rDNA CN may have been affected by the mutation itself, since 10% of gene deletions in *S. cerevisiae* result in a change in the number of repeats within the chromosomal rDNA array (19, 34, 42). Third, growth or metabolic conditions can modulate the size of the chromosomal rDNA locus. For instance, the rDNA array reaches different sizes depending on the environmental conditions (20), a phenomenon that was also observed in *Drosophila* (16). Thus, by comparing individual wild-type and mutant strains the contribution of a gene deletion to lifespan could easily be confused with a copy number effect and the accurate interpretation of lifespan data must account for rDNA CN. Given the current accessibility of next-generation sequencing, we envision that rDNA CN will be a necessary parameter to quantify and consider when conducting yeast RLS experiments.

As noted in the Introduction, the chromosomal rDNA array is a type of "contingency locus" that responds to cellular dynamics and environment to allow the cell to adapt to changes in its metabolic state (14). This has at least two implications: First, growth conditions and genetics can have a large impact on the RLS of a strain through modulation of rDNA CN. Second, this provides an example of antagonistic pleiotropy, as hypothesized by Williams (43). Mansisidor et al. (13) proposed that the presence of ERCs associated with short rDNA arrays provides metabolic flexibility in young cells. However, having an abundance of ERCs in young cells becomes a burden later in life.

Similar mechanisms to those reported here may be at play in metazoan systems. Prior work has demonstrated that there is extensive rDNA CN variation at both the population and single-cell level and that pathways regulating this process are conserved between yeast and mammals (44–46). It has also been demonstrated that nutritional stresses and aging can affect the level of copy number and DNA methylation of fly, mouse, and human rDNA (47–49). Importantly, variation in rDNA CN within these organisms has phenotypic consequences, including effects on mitochondrial copy number and transcriptional signatures (50). Given these findings, we suggest that rDNA loci, specifically their copy number variations, warrant further investigation into their regulation of aging in mammalian systems.

Materials and Methods

Yeast Strains and Media Conditions. All strains are in the S288C strain background (25). Strains derived directly from BY4743 were obtained by sporulation. To introduce variability in rDNA length, BY4743 was transformed with a linearized construct that contained a HYG cassette flanked by homology to the NTS1 and NTS2 regions of the rDNA repeat. This construct was analogous to the one published by Mansisidor et al. (13). To construct all other strains, a *MATa* and *MAT*α clone, which was obtained by backcrossing the wild type of the prototrophic deletion collection (*can1*Δ ::STE2pr-spHIS5 *his3*Δ *1 lyp1*Δ *0*) (51) with BY4741, was used. Genes of interest were knocked out in the resulting diploid and then sporulated. This was sufficient to introduce some variability in rDNA array length in this strain. To obtain more extreme CN variations, the HYG construct mentioned above was used.

All experiments were performed in synthetic complete (SC) medium, unless indicated otherwise. SC medium contained 1× SC mix and 1× yeast nitrogen base (YNB) with ammonium sulfate (Sunrise Science), 2% glucose, and 2% methyl-alpha-D-mannopyranoside (MMP) (Sigma Aldrich), pH 4.5. Minimal media (YNB) were identical to SC except without the 1× SC mix. rich media, yeast extract peptone dextrose (YPD), contained 1% wt/vol yeast extract, 2% wt/vol Bacto peptone, and 2% glucose. For aging experiments in the modified MAD system, SC medium with two modifications was used: biotin-free YNB (Sunrise Science) and additional 40 mM 7,8-diaminopelargonic acid (DAPA) (27).

Cell Size and Growth Rate Measurements. Growth rate measurements were obtained from cells grown to saturation in SC overnight and then diluted to optical density 600 nm (OD) 0.01. OD was measured at 2, 3, 4, 5, 6, 7, 8, 10, 12 and 14 h after dilution. Cell size was measured in triplicate on cells grown in SC medium for 24 h at low OD (<0.05), using a Multisizer 4e Coulter Counter (Beckman Coulter).

Replicative Lifespan Measurements. Replicative lifespan measurements were made as described in Thayer et al. (1). Briefly, cells were grown to saturation in the respective medium type in 24-well plates and then grown for 24 h below an OD 0.05. Cells were then loaded into microfluidics devices specifically designed to retain aging mother cells in polydimethylsiloxane cell "catchers." Brightfield images were collected every 15 min for 96 h. Time-lapse images were analyzed by an automated computer vision pipeline, predicting number of divisions as well as death vs. censoring for each cell in the catchers. Median lifespan was estimated using the Kaplan–Meier estimate of the survival function. Model performance was validated by manual annotation of a subset of the images used in this study (*SI Appendix*, Fig. S10). A microdissection assay was performed as previously described (26).

Aging of Bulk Cell Populations in a Modified MAD System. To obtain large amounts of aged cells, $\sim 10^9$ cells for each strain were grown in biotin-free SC medium that contained the biotin precursor DAPA. Cultures were grown at an OD <0.05 for 24 h. Using this medium instead of regular SC prevents competition between free biotin in the medium and biotinylated cells (27). Cells were harvested and washed three times with 1× PBS and then incubated with 0.5 mg Sulfo-NHS-LC-LC-Biotin (Sigma Aldrich) per 2.5×10^7 cells for 30 min. Biotinylated cells were then washed three times with medium and recovered at 30 °C in medium for 6 h at OD <0.05. Then, 22.5 mg of Dynabeads MyOne Streptavidin C1 magnetic beads (65001; Thermo Fisher) per 2.5×10^7 cells were added directly to the flasks and incubated for 10 min with occasional swirling. Next, cells were collected on a 0.22-μm filter (431098; Corning) and beaded mother cells were purified by sequential washing on a DynaMag-2 magnet (Invitrogen). Finally, cells were loaded into a modified MAD (27) prefilled with medium and allowed to bind to the magnets for 5 min before the peristaltic media pumps were turned on. This system has the same basic setup as the original MAD with a glass vessel, a metallic bubble cage, circular magnets on the outside of the vessel, and three media ports (for cell loading, media influx, and media outflux). However, the dimensions of the vessel in this version of the MAD (130 mL media content) allow loading of 10^9 cells per device and thicker peristaltic marprene tubing (978.0102.00+; Watson Marlow) enables increased media flow. After 24 h, $\sim 6 \times 10^8$ cells per sample were harvested.

ERC Blots. Bulk genomic DNA was extracted using a protocol similar to that in Mansisidor et al. (13). In brief, $\sim 6 \times 10^8$ cells were spun down, washed in nuclease-free H_2O, and resuspended in 800 μL digestion buffer (1 M Sorbitol, 42 mM K_2HPO_4, 8 mM KH_2PO_4, 5 mM ethylenediaminetetraacetic acid (EDTA)) containing 40 μL R-Zymolyase (Zymo Research). After incubation at 37 °C for 1 h, 1,140 μL Proteinase K (Qiagen) and 44 μL 10% sodium dodecyl sulfate (SDS) were added. Lysates were incubated at 65 ° C for 1.5 h with occasional stirring. Next, SDS was precipitated out by addition of 1/10 vol of 3 M potassium acetate (pH 5.5) and centrifuged at 21,000 × *g* for 10 min. Totals of 1/10 vol of 3 M sodium acetate (pH 5.5) and 2 vol of 100% ethanol were added and DNA was precipitated for 1 h at −20 °C. DNA was spun down at 21,000 × *g* for 10 min and washed two times with 75% ethanol. Pellets were resuspended in nuclease-free H_2O and genomic DNA was quantified with the Qubit dsDNA Broad Range kit (Invitrogen).

Equal amounts of DNA (1.5 μg total) were digested with BamHI overnight and then run on a 0.7% agarose gel at 35 V for 20 h. To control for loading, equal amounts of sample were loaded on a separate 0.7% agarose gel, which ran for 4 h. For Southern blotting, gels were washed sequentially (0.25 M HCl; 0.5 N NaOH and 1 M NaCl; 0.5 M Tris [pH 7] and 3 M NaCl) for 2 × 15 min each and then blotted overnight onto a nylon membrane (NJ0HY00010; GE Water & Process Technologies). Then, DNA was cross-linked in a UV Stratalinker 2400 (Stratagene) and then hybridized overnight at 42 °C with radioactive P^{32}-labeled probe against *RDN25* and *NPR2*, respectively. *RDN25* probe was made by PCR with oligos 5′-TATTTCACTGGCGCCGAAGCTCCCA-3′ and 5′-TACGGACAAGGGGAATCTGACTGT-3′ on pDL05 as template (28). *NPR2* probes were made with oligos 5′-CTATCACTTGTTGCCTGTATCTC-3′ and 5′-CTAGGATTTGGCGTGGATGAA-3′ on the *NPR2* vector from the centromere-based molecular barcoded yeast plasmid collection (52). Blots were used to expose storage phosphor screens, which were then imaged on a Typhoon FLA 9500 (GE Healthcare).

Whole-Genome Sequencing and Copy Number Estimation. Cells were grown to saturation in YPD overnight in 24-well plates and washed one time with H_2O, and then genomic DNA was extracted using the YeaStar Genomic DNA kit (D2002; Zymo Research). The input sample was normalized to 60 ng and fed into the Illumina DNA prep kit (20018705; Illumina) for transposition-based library preparation per vendor's instructions using six cycles of PCR. The resulting libraries were quality controlled and quantified on a Fragment Analyzer (Agilent) using the 50-kb extended-ladder Genomic DNA kit (DNF-467-0500; Agilent). Libraries were pooled at equal concentrations and sequenced on the Illumina NovaSeq with 150 bp paired-end reads. Reads were aligned to the *S. cerevisiae* genome (sacCer3, Release 64) using bowtie2 version 2.3.5.1 with default parameters. Sequence variations were called using the bcftools software package. Copy number was estimated by calculating the average read depth at three locations on chromosome 12 (Chr12): two single-copy loci (Chr12:760,000..790,000 and Chr12:160,000..190,000) and one in the rDNA locus (Chr12:451,575..468,931). Copy number was estimated to be the following: median(rDNA locus depth)/mean[median(Chr12-L1 depth), median(Chr12-L2 depth)]. Samples with large GC sequencing bias were excluded.

CHEF Gels. Approximately 10^8 cells per sample were resuspended in 50 mM EDTA and then mixed with 1% low-melt agarose (SeaPlaque GTG agarose; Lonza) in 50 mM EDTA. The agarose/cell mix was transferred to CHEF Disposable Plug Molds (1703713; Bio-Rad) and cooled for 15 min at 4 °C. Plugs were incubated for 4 h at 37 °C in 1 mL of spheroplasting solution (1 M Sorbitol, 10 mM Tris·HCl [pH 8.0], 14 mM beta-mercaptoethanol, 20 mM EDTA, 0.5 mg/mL Zymolyase) and then washed for 15 min in LDS solution (1% lithium dodecyl sulfate, 10 mM Tris·HCl [pH 8.0], 100 mM EDTA). Plugs were then incubated overnight in fresh LDS solution at 37 °C, washed three times for 20 min with NDS solution (2 mM Tris base [pH 9.5], 1% Sarcosyl, 100 mM EDTA), and then washed five times with Tris (10 mM) EDTA (1 mM) (pH 8.0). For the digest, plugs were washed three times for 20 min with 1 mL 1× NEB Buffer 4 + 1× BSA (New England Biolabs) and then covered with 50 μL digestion solution (1.3 μL BamHI-HF, 1× NEB Buffer 4, 1× BSA) and incubated for 5 h at 37 °C.

For gel casting, 0.8% low electroendosmosis agarose (SeaKem LE Agarose; Lonza) was melted in 0.5× Tris–borate–EDTA buffer (TBE; 1×: 45 mM Tris, 45 mM borate, 1 mM EDTA) and kept at 50 °C. Plugs, including one with *Hansenula wingei* standard ladder (170-3667; Bio-Rad), were transferred onto the gel comb and excess liquid was dried off with a Kimwipe. The comb was then carefully placed into the casting tray and melted agarose was poured around it. Once the gel was solidified, it was transferred into a CHEF gel module (CHEF-DRII; Bio-Rad) containing 0.5× TBE buffer. The gel was run for 32 h with settings optimized for a size range of 0.44 to 2.3 Mb. Southern blot was performed as above, except the probes were made by PCR with digoxigenin-labeled dUTP using *RDN25* oligos as above (11277065910; Roche). Blots were probed with Anti-Digoxigenin-AP Fab fragments (11093274910; Roche) and visualized with CDP-Star (11685627001; Roche).

RNA Extraction. Samples were processed similarly to that described in Hendrickson et al. (27). Frozen cell pellets ($\sim 10^7$) were resuspended in 200 μL of

Lysis buffer (10 mM Tris [pH 8.0], 0.5% SDS, 10 mM EDTA). Following the addition of 200 μL acid phenol (pH 4.3), samples were vortexed for 30 s. Samples were incubated at 65 °C for 30 min in a thermomixer with intermittent shaking (2,000 rpm for 1 min every 15 min). A total of 400 μL of ethanol was then added and the RNA was purified using the Direct-zol RNA Miniprep Plus kit (R2071; Zymo Research) according to the manufacturer's protocol, including the optional DNase digestion step. RNA integrity was confirmed using an Agilent Bioanalyzer.

RNA-Seq Library Preparation. RNA-Seq libraries were processed similarly to that described in Hendrickson et al. (27). No-selection libraries were generated using the NEBNext Ultra II Directional RNA Library Prep Kit (PNE7760L; Illumina) without the polyA selection step. Given the concentration of RNA is much higher for total unselected RNA, 10 ng of total RNA was input and the fragmentation time was increased to 20 min (vs. 15 min standard) to ensure efficient fragmentation of rRNA and proceeded with the vendor's protocol. Traditional RNA-Seq libraries were generated using the NEBNext Ultra II Directional RNA Library Prep Kit using 250 ng of input and vendor's protocol with polyA selection. All libraries were sequenced on an Illumina NOVASEQ with 150 × 150 paired-end reads.

RNA-Seq Data Processing and Analysis. RNA-Seq data were quantified using Salmon-0.8.1 with two separate annotation indexes, as described in ref. 27:

- open-reading frames (ORFs) as defined by *Saccharomyces* Genome Database (SGD); and
- "complex transcriptome" index created by aggregating ORFs, their longest annotated untranslated regions (UTRs), and all noncanonical and noncoding transcripts pulled from SGD

Salmon was run using the "quant" command with the following settings: "--libType ISR --useVBOpt [ ] --numBootstraps 30 --incompatPrior 0."

Salmon quantification was prepared and processed for differential expression analysis using Tximport (53). Differential gene expression analysis was performed with DESEQ2 using a Wald test and replicative lifespan as a numeric variable.

ATAC-Seq Sample Preparation. ATAC-Seq samples were processed similarly to that described in Hendrickson et al. (27). For each sample, ∼5 × 10^6 cells were spun down at 1,200 × *g* for 4 min and resuspended in 250 μL media. Cells were washed twice with SB buffer (1 M Sorbitol, 40 mM Hepes [pH 7.5], 10 mM $MgCl_2$) and then resuspended in 190 μL SB Buffer. A total of 10 μL of 10 mg/mL Zymolyase100T was added and cells were incubated at 30 °C for 30 min while shaking (600 rpm) in a thermomixer (Eppendorf). Spheroplasts were spun down at 1,500 × *g* for 5 min, washed twice with SB Buffer, resuspended in 50 μL Tagmentation Mix (25 μL Nextera Tagment DNA Buffer, 22.5 μL H_2O, 2.5 μL Nextera Tagment DNA Enzyme I), and incubated at 37 °C for 30 min. DNA was purified over DNA Clean and Concentrator-5 kit columns (D4013; Zymo Research) following the manufacturer's protocol, eluted in 11 μL H_2O, and stored at −20 °C until ready for PCR.

PCR reactions were set up using Nextera Index i5 and i7 series PCR primers (Illumina). Totals of 25 μL NEBNext Hi-Fidelity 2× PCR Master Mix, 7.5 μL H_2O, 6.25 μL i5 primer (10 μM), 6.25 μL i7 primer (10 μM), and 5 μL tagmented DNA from above were mixed, such that each sample had a unique barcoded primer pair. PCR amplification was run (72 °C for 5 min and 98 °C for 30 s; eight cycles of 98 °C for 10 s, 63 °C for 30 s, 72 °C for 1 min; and hold at 4 °C). PCR reactions were cleaned up over DNA Clean and Concentrator-5 columns to eliminate primers (D4013; Zymo Research), eluted in 22 μL H_2O, analyzed on the BioAnalyzer, and size selected for fragments between 150 and 600 bp using a Pippin Prep (Sage Science).

ATAC-Seq Data Analysis. Raw ATAC-Seq data were processed similarly to that described in Hendrickson et al. (27). Briefly, the raw paired-end reads were aligned to the *S. cerevisiae* genome (sacCer3, Release 64) using bowtie2 version 2.3.5.1 with default parameters. Second, the alignments were filtered, requiring that both reads in the pair are mapped concordantly, using the "0 × 2" flag in samtools. Third, the alignments were converted to track the number of insertions at each position in the genome. For every aligned fragment, the insertion locations are calculated by shifting the fragment ends of reads that align to the "+" strand by four nucleotides and shifting the fragment ends of reads that align to the "−" strand by five nucleotides in the 3′ direction to reflect the distance to the center of the transposase binding site (54). To normalize for unequal sequencing depth, insertion counts were normalized by the total number of reads in each sample.

Mode-of-Death Automated Analysis. To classify the mode of death, 30 frames from each side of the predicted death mode location were extracted for a total of 61 frames. The frames were padded with zero if the boundary extended out of the movie. The data were fed into a deep neural network as shown in the graph in *SI Appendix*, Fig. S6*B*. The main feature extraction network was a pretrained resnet50 model on Imagenet with the following modifications:

- The first convolution layer was modified to accept a single-channel input image.
- The classification layer was replaced with an output of 256 classes.

Once the images passed through the convolutional layer, the extracted features were flattened into two dimensions (2D), and additional sets of one-dimensional (1D) convolution and maxpooling were performed. The outputs were averaged along the frame dimension and fed into a fully connected layer to produce the logits for mode classification. Performance of the model was assessed by manual annotation of a subset of lifespan movies. Comparisons of manual annotations and predictions are summarized in *SI Appendix*, Fig. S6 *C*–*E*.

Cox Proportional Hazard Analysis. The effect of each variable on hazard/survival was estimated by fitting a Cox Proportional Hazard model with the lifelines software package (55). The equation can be described as follows:

$$h(t) = b_0(t) \cdot (PH_r + PH_e + PH_m + PH_i) \quad [1]$$

$$PH_r = \exp(b_{r_1} \cdot rDNA_1) + \exp(b_{r_2} \cdot rDNA_2) \quad [2]$$

$$PH_e = \exp(\sum_{i=1}^{n} b_i \cdot e_i) \quad [3]$$

$$PH_m = \exp(\sum_{j=1}^{n} b_j \cdot mut_j) \quad [4]$$

$$PH_i = \exp(\sum_{j=1}^{n} b_{jr} \cdot mut_j \cdot rDNA_1). \quad [5]$$

Eq. **1** defines the complete hazard function, where the baseline hazard is scaled by the sum of a number of partial hazards, described in Eqs. **2**–**5**. Eq. **2** describes the effects of rDNA CN, modeled as two factors–the number of repeats above/below a normal copy number of 150 ($rDNA_1$ and $rDNA_2$, respectively). The resulting piecewise linear fit allowed the model to capture the nonlinearity observed above 150 repeats. Eq. **3** describes the contribution of any experiment-to-experiment batch effects. Eq. **4** describes the contribution of any particular mutation. Eq. **5** describes the interaction terms between rDNA CN ($rDNA_1$ /below 150) and mutations that are shown in Fig. 4 *H*, *Right* (*fob1*Δ, *hda2*Δ, *upb8*Δ, *ubr2*Δ). *b* terms in Eqs. **3**–**5** were set to 0 for initial characterization of WT panel and were fitted only while determining the effects of various mutants (Fig. 4).

Data Availability. Code and data used to generate the figures are available on GitHub at https://github.com/calico/rDNAcn (56). Description of the strains used in this study and data used to generate figures (e.g., cell and growth measurements, gel quantification, and statistical analyses) are available in Dataset S1. Raw and processed images have been archived and can be made available upon request. Whole-genome sequencing is deposited at the NCBI Sequencing Read Archive (PRJNA796586) (57). RNA-Seq and ATAC-Seq data are deposited at the Gene Expression Omnibus (GSE193600) (58).

ACKNOWLEDGMENTS. We thank Michael Robles for production of the microfluidics devices used in this study; Hannah DeBaets, Twaritha Vijay, and other members of the Calico Genomics Group for whole-genome sequencing developments; Jason Rogers for annotation of data used during training of the mode-of-death computer vision model and discussions about competing hazard analysis; Bernd Wranik for initial strain construction; and members of the Gottschling laboratory, Anastasia Baryshnikova, David Botstein, and Jacob Kimmel for critical reading of the manuscript. Fig. 5 was created with BioRender.com.

1. N. H. Thayer *et al.*, The yeast lifespan machine: A microfluidic platform for automated replicative lifespan measurements. bioRxiv [Preprint] (2022). https://www.biorxiv.org/content/10.1101/2022.02.14.480146v1 (Accessed 15 February 2022).
2. S. S. Lee, I. Avalos Vizcarra, D. H. Huberts, L. P. Lee, M. Heinemann, Whole lifespan microscopic observation of budding yeast aging through a microfluidic dissection platform. *Proc. Natl. Acad. Sci. U.S.A.* **109**, 4916–4920 (2012).
3. Z. Xie *et al.*, Molecular phenotyping of aging in single yeast cells using a novel microfluidic device. *Aging Cell* **11**, 599–606 (2012).
4. M. C. Jo, W. Liu, L. Gu, W. Dang, L. Qin, High-throughput analysis of yeast replicative aging using a microfluidic system. *Proc. Natl. Acad. Sci. U.S.A.* **112**, 9364–9369 (2015).
5. Y. Li *et al.*, Multigenerational silencing dynamics control cell aging. *Proc. Natl. Acad. Sci. U.S.A.* **114**, 11253–11258 (2017).
6. A. Denoth Lippuner, T. Julou, Y. Barral, Budding yeast as a model organism to study the effects of age. *FEMS Microbiol. Rev.* **38**, 300–325 (2014).
7. D. A. Sinclair, L. Guarente, Extrachromosomal rDNA circles–A cause of aging in yeast. *Cell* **91**, 1033–1042 (1997).
8. M. Kaeberlein, M. McVey, L. Guarente, The SIR2/3/4 complex and SIR2 alone promote longevity in *Saccharomyces cerevisiae* by two different mechanisms. *Genes Dev.* **13**, 2570–2580 (1999).
9. T. Kobayashi, T. Horiuchi, A yeast gene product, Fob1 protein, required for both replication fork blocking and recombinational hotspot activities. *Genes Cells* **1**, 465–474 (1996).
10. T. Kobayashi, D. J. Heck, M. Nomura, T. Horiuchi, Expansion and contraction of ribosomal DNA repeats in *Saccharomyces cerevisiae*: Requirement of replication fork blocking (Fob1) protein and the role of RNA polymerase I. *Genes Dev.* **12**, 3821–3830 (1998).
11. P. A. Defossez *et al.*, Elimination of replication block protein Fob1 extends the life span of yeast mother cells. *Mol. Cell* **3**, 447–455 (1999).
12. E. X. Kwan, X. S. Wang, H. M. Amemiya, B. J. Brewer, M. K. Raghuraman, rDNA copy number variants are frequent passenger mutations in *Saccharomyces cerevisiae* deletion collections and de novo transformants. *G3 (Bethesda)* **6**, 2829–2838 (2016).
13. A. Mansisidor *et al.*, Genomic copy-number loss is rescued by self-limiting production of DNA circles. *Mol. Cell* **72**, 583–593.e4 (2018).
14. O. J. Rando, K. J. Verstrepen, Timescales of genetic and epigenetic inheritance. *Cell* **128**, 655–668 (2007).
15. A. H. Michel, B. Kornmann, K. Dubrana, D. Shore, Spontaneous rDNA copy number variation modulates Sir2 levels and epigenetic gene silencing. *Genes Dev.* **19**, 1199–1210 (2005).
16. J. C. Aldrich, K. A. Maggert, Transgenerational inheritance of diet-induced genome rearrangements in *Drosophila*. *PLoS Genet.* **11**, e1005148 (2015).
17. D. Sharma *et al.*, A new method for determining ribosomal DNA copy number shows differences between Saccharomyces cerevisiae populations. bioRxiv [Preprint] (2021). https://www.biorxiv.org/content/10.1101/2021.01.21.427686v3 (Accessed 17 February 2021).
18. K. Saka, S. Ide, A. R. Ganley, T. Kobayashi, Cellular senescence in yeast is regulated by rDNA noncoding transcription. *Curr. Biol.* **23**, 1794–1798 (2013).
19. F. Puddu *et al.*, Genome architecture and stability in the *Saccharomyces cerevisiae* knockout collection. *Nature* **573**, 416–420 (2019).
20. C. V. Jack *et al.*, Regulation of ribosomal DNA amplification by the TOR pathway. *Proc. Natl. Acad. Sci. U.S.A.* **112**, 9674–9679 (2015).
21. T. Iida, T. Kobayashi, RNA polymerase I activators count and adjust ribosomal RNA gene copy number. *Mol. Cell* **73**, 645–654.e13 (2019).
22. D. H. Huberts *et al.*, Calorie restriction does not elicit a robust extension of replicative lifespan in *Saccharomyces cerevisiae*. *Proc. Natl. Acad. Sci. U.S.A.* **111**, 11727–11731 (2014).
23. M. A. McCormick *et al.*, A comprehensive analysis of replicative lifespan in 4,698 single-gene deletion strains uncovers conserved mechanisms of aging. *Cell Metab.* **22**, 895–906 (2015).
24. D. E. Gottschling, T. Nyström, The upsides and downsides of organelle interconnectivity. *Cell* **169**, 24–34 (2017).
25. C. B. Brachmann *et al.*, Designer deletion strains derived from *Saccharomyces cerevisiae* S288C: A useful set of strains and plasmids for PCR-mediated gene disruption and other applications. *Yeast* **14**, 115–132 (1998).
26. K. K. Steffen, B. K. Kennedy, M. Kaeberlein, Measuring replicative life span in the budding yeast. *J. Vis. Exp.* (2009).
27. D. G. Hendrickson *et al.*, A new experimental platform facilitates assessment of the transcriptional and chromatin landscapes of aging yeast. *eLife* **7**, e39911 (2018).
28. D. L. Lindstrom, C. K. Leverich, K. A. Henderson, D. E. Gottschling, Replicative age induces mitotic recombination in the ribosomal RNA gene cluster of *Saccharomyces cerevisiae*. *PLoS Genet.* **7**, e1002015 (2011).
29. M. Jin *et al.*, Divergent aging of isogenic yeast cells revealed through single-cell phenotypic dynamics. *Cell Syst.* **8**, 242–253.e3 (2019).
30. Y. Li *et al.*, A programmable fate decision landscape underlies single-cell aging in yeast. *Science* **369**, 325–329 (2020).
31. J. Yang *et al.*, Cell size and growth rate are major determinants of replicative lifespan. *Cell Cycle* **10**, 144–155 (2011).
32. C. He *et al.*, Enhanced longevity by ibuprofen, conserved in multiple species, occurs in yeast through inhibition of tryptophan import. *PLoS Genet.* **10**, e1004860 (2014).
33. E. X. Kwan *et al.*, Coordination of genome replication and anaphase entry by rDNA copy number in *S. cerevisiae*. bioRxiv [Preprint] (2021). https://www.biorxiv.org/content/10.1101/2021.02.25.432950v2 (Accessed 15 April 2021).
34. K. Saka, A. Takahashi, M. Sasaki, T. Kobayashi, More than 10% of yeast genes are related to genome stability and influence cellular senescence via rDNA maintenance. *Nucleic Acids Res.* **44**, 4211–4221 (2016).
35. G. Giaever *et al.*, Functional profiling of the *Saccharomyces cerevisiae* genome. *Nature* **418**, 387–391 (2002).
36. M. Kaeberlein, K. T. Kirkland, S. Fields, B. K. Kennedy, Sir2-independent life span extension by calorie restriction in yeast. *PLoS Biol.* **2**, E296 (2004).
37. M. Kaeberlein *et al.*, Regulation of yeast replicative life span by TOR and Sch9 in response to nutrients. *Science* **310**, 1193–1196 (2005).
38. E. D. Smith *et al.*, Quantitative evidence for conserved longevity pathways between divergent eukaryotic species. *Genome Res.* **18**, 564–570 (2008).
39. K. K. Steffen *et al.*, Yeast life span extension by depletion of 60s ribosomal subunits is mediated by Gcn4. *Cell* **133**, 292–302 (2008).
40. U. Kruegel *et al.*, Elevated proteasome capacity extends replicative lifespan in *Saccharomyces cerevisiae*. *PLoS Genet.* **7**, e1002253 (2011).
41. R. Yu *et al.*, Inactivating histone deacetylase HDA promotes longevity by mobilizing trehalose metabolism. *Nat. Commun.* **12**, 1981 (2021).
42. M. P. Andersen, Z. W. Nelson, E. D. Hetrick, D. E. Gottschling, A genetic screen for increased loss of heterozygosity in *Saccharomyces cerevisiae*. *Genetics* **179**, 1179–1195 (2008).
43. G. C. Williams, Pleiotropy, natural selection, and the evolution of senescence. *Evolution* **11**, 398–411 (1957).
44. M. M. Parks *et al.*, Variant ribosomal RNA alleles are conserved and exhibit tissue-specific expression. *Sci. Adv.* **4**, eaao0665 (2018).
45. M. van Sluis, C. van Vuuren, H. Mangan, B. McStay, NORs on human acrocentric chromosome p-arms are active by default and can associate with nucleoli independently of rDNA. *Proc. Natl. Acad. Sci. U.S.A.* **117**, 10368–10377 (2020).
46. S. Paredes *et al.*, The epigenetic regulator SIRT7 guards against mammalian cellular senescence induced by ribosomal DNA instability. *J. Biol. Chem.* **293**, 11242–11250 (2018).
47. M. L. Holland *et al.*, Early-life nutrition modulates the epigenetic state of specific rDNA genetic variants in mice. *Science* **353**, 495–498 (2016).
48. K. L. Lu, J. O. Nelson, G. J. Watase, N. Warsinger-Pepe, Y. M. Yamashita, Transgenerational dynamics of rDNA copy number in *Drosophila* male germline stem cells. *eLife* **7**, e32421 (2018).
49. P. D'Aquila *et al.*, Methylation of the ribosomal RNA gene promoter is associated with aging and age-related decline. *Aging Cell* **16**, 966–975 (2017).
50. J. G. Gibbons, A. T. Branco, S. Yu, B. Lemos, Ribosomal DNA copy number is coupled with gene expression variation and mitochondrial abundance in humans. *Nat. Commun.* **5**, 4850 (2014).
51. P. A. Gibney, C. Lu, A. A. Caudy, D. C. Hess, D. Botstein, Yeast metabolic and signaling genes are required for heat-shock survival and have little overlap with the heat-induced genes. *Proc. Natl. Acad. Sci. U.S.A.* **110**, E4393–E4402 (2013).
52. C. H. Ho *et al.*, A molecular barcoded yeast ORF library enables mode-of-action analysis of bioactive compounds. *Nat. Biotechnol.* **27**, 369–377 (2009).
53. C. Soneson, M. I. Love, M. D. Robinson, Differential analyses for RNA-seq: Transcript-level estimates improve gene-level inferences. *F1000 Res.* **4**, 1521 (2015).
54. J. D. Buenrostro, P. G. Giresi, L. C. Zaba, H. Y. Chang, W. J. Greenleaf, Transposition of native chromatin for fast and sensitive epigenomic profiling of open chromatin, DNA-binding proteins and nucleosome position. *Nat. Methods* **10**, 1213–1218 (2013).
55. C. Davidson-Pilon, lifelines: Survival analysis in python. *J. Open Source Softw.* **4**, 1317 (2019).
56. M. Hotz *et al.*, rDNAcn. GitHub. https://github.com/calico/rDNAcn. Accessed 22 March 2022.
57. M. Hotz *et al.*, rDNA array length is a major determinant of replicative lifespan in budding yeast - WGS data. Sequence Read Archive. https://www.ncbi.nlm.nih.gov/sra/PRJNA796586. Deposited 12 January 2022.
58. M. Hotz *et al.*, rDNA array length is a major determinant of replicative lifespan in budding yeast. Gene Expression Omnibus. https://www.ncbi.nlm.nih.gov/geo/query/acc.cgi?acc=GSE193600. Deposited 13 January 2022.